Structure and Dynamics of a Phase-Separating Active Colloidal Fluid

Gabriel S. Redner, Michael F. Hagan,* and Aparna Baskaran†

Martin Fisher School of Physics, Brandeis University, Waltham, Massachusetts, USA
(Received 6 July 2012; published 31 January 2013)

We examine a minimal model for an active colloidal fluid in the form of self-propelled Brownian spheres that interact purely through excluded volume with no aligning interaction. Using simulations and analytic modeling, we quantify the phase diagram and separation kinetics. We show that this nonequilibrium active system undergoes an analog of an equilibrium continuous phase transition, with a binodal curve beneath which the system separates into dense and dilute phases whose concentrations depend only on activity. The dense phase is a unique material that we call an active solid, which exhibits the structural signatures of a crystalline solid near the crystal-hexatic transition point, and anomalous dynamics including superdiffusive motion on intermediate time scales.

Active fluids composed of self-propelled units occur in nature on many scales ranging from cytoskeletal filaments and bacterial suspensions to macroscopic entities such as insects, fish, and birds [1]. These systems exhibit strange and exciting phenomena such as dynamical self-regulation [2], clustering [3], anomalous density fluctuations [4], unusual rheological behavior [5–7], and activity-dependent phase boundary changes [8]. Motivated by these findings, recent experiments have focused on realizing active fluids in nonliving systems, using chemically propelled particles undergoing self-diffusophoresis [9–11], Janus particles undergoing thermophoresis [12,13], as well as vibrated monolayers of granular particles [14–16].

In this Letter we explore a minimal active fluid model: a system of self-propelled smooth spheres interacting by excluded volume alone and confined to two dimensions. Unlike self-propelled rods [17–21], these particles cannot interchange angular momentum and thus lack a mutual alignment mechanism. Recent simulation and experimental studies have shown that this system exhibits giant number fluctuations [22] and athermal phase separation [22,23] that are characteristic of active fluids [4,24,25]. Here we employ extensive Brownian dynamics simulations to characterize the phase diagram of this system and we develop an analytic model that captures its essential features. We show that this nonequilibrium system undergoes a continuous phase transition, analogous to that of equilibrium systems with attractive interactions, and that the phase separation kinetics demonstrate equilibriumlike coarsening. These structural and dynamic signatures of phase separation and coexistence enable an unequivocal definition of phases in this nonequilibrium, active system. Finally, we find that the dense phase is a dynamic new form of material that we call an "active solid." This material exhibits structural properties consistent with a 2D colloidal crystal near the crystal-hexatic transition point [26,27], but is characterized by such anomalous features as

superdiffusive transport at intermediate time scales and a heterogeneous and dynamic stress distribution (see Fig. 1).

Model and simulation method.—Our system consists of smooth spheres immersed in a solvent and confined to a
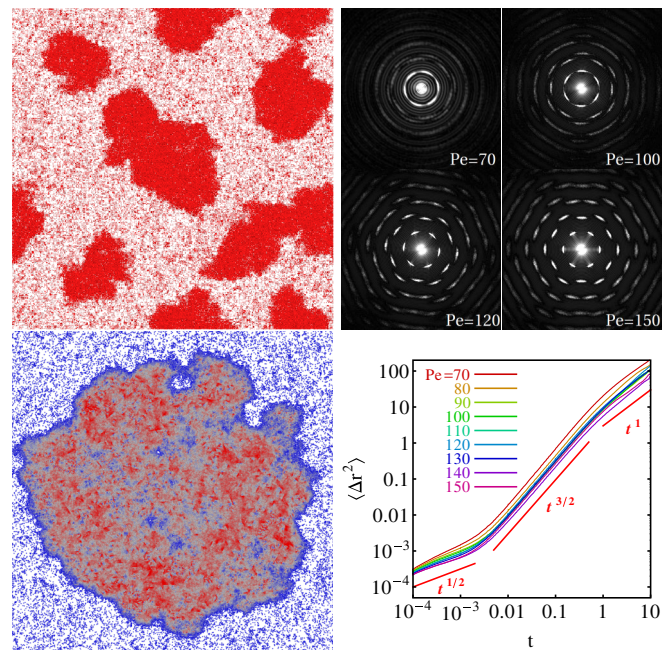

FIG. 1 (color online). A visual summary of our results. Top left: beyond critical density and activity levels the active colloidal fluid separates into dense and dilute phases. The clusters coarsen over time (see S1 in the Supplemental Material in [34]). Top right: the static structure factor $S(\boldsymbol{k}) = \frac{1}{N}\langle\sum_{ij}e^{i\boldsymbol{k}\cdot\boldsymbol{r}_{ij}}\rangle$, restricted to the interiors of large clusters. These signatures resemble those of a high temperature colloidal crystal near the crystal-hexatic phase transition. Bottom left: a heat map of the pressure in the active solid material. It is heterogeneous and highly dynamic, indicating that external stresses would produce a complex response. Bottom right: log-log plot of the mean square displacement of a tagged particle in the active solid. At intermediate time scales, it exhibits anomalous superdiffusive transport.

plane, similar to experimental systems of self-propelled colloids sedimented at an interface [23]. Each particle is self-propelled with a constant force, and interactions between particles result from isotropic excluded-volume repulsion only. We include no mechanism for explicit alignment or transmission of torques between particles.

The state of the system is represented by the positions and self-propulsion directions $\{\mathbf{r}_i, \theta_i\}_{i=1}^N$ of all particles. Their evolution is governed by the coupled overdamped Langevin equations,

$$\dot{\mathbf{r}}_i = D\beta[\mathbf{F}_{\text{ex}}(\{\mathbf{r}_i\}) + F_p\hat{\boldsymbol{\nu}}_i] + \sqrt{2D}\boldsymbol{\eta}_i^T, \quad (1)$$

$$\dot{\theta}_i = \sqrt{2D_r}\eta_i^R. \quad (2)$$

Here, $\mathbf{F}_{\text{ex}}$ is an excluded-volume repulsive force given by the WCA potential $V_{\text{ex}} = 4\epsilon[(\frac{\sigma}{r})^{12} - (\frac{\sigma}{r})^6] + \epsilon$ if $r < 2^{(1/6)}$, and zero otherwise [28], with σ the nominal particle diameter. We use $\epsilon = k_BT$, but our results should be insensitive to the exact strength and form of the potential. F_p is the magnitude of the self-propulsion force which, in the absence of interactions, will move a particle with speed $v_p = D\beta F_p$, $\hat{\boldsymbol{\nu}}_i = (\cos\theta_i, \sin\theta_i)$, and $\beta = \frac{1}{k_BT}$. D and D_r are translational and rotational diffusion constants, which in the low-Reynolds-number regime are related by $D_r = \frac{3D}{\sigma^2}$. The η are Gaussian white noise variables with $\langle\eta_i(t)\rangle = 0$ and $\langle\eta_i(t)\eta_j(t')\rangle = \delta_{ij}\delta(t - t')$.

We nondimensionalized the equations of motion using σ and k_BT as basic units of length and energy, and $\tau = \frac{\sigma^2}{D}$ as the unit of time. Simulations employed the stochastic Runge-Kutta method [29] with maximum time step $2 \times 10^{-5}\tau$. Simulations mapping the phase diagram were run with 15 000 particles until time 100τ, while larger systems (up to 512 000 particles) were used to explore kinetics and material properties. The simulation box was square with periodic boundaries, with its size chosen to achieve the desired density. The system is parametrized by two dimensionless values, the packing fraction ϕ and the Péclet number, which in our units is identical to the nondimensionalized velocity ($\text{Pe} = v_p\frac{\tau}{\sigma}$). In this work, we varied ϕ from near zero to the hard-sphere close-packing value $\phi_{\text{cp}} = \frac{\pi}{2\sqrt{3}}$, and Pe from zero to 150.

Phase separation.—We first show that our results are consistent with prior simulations [22] and confirm that this system, despite the absence of aligning interactions, shows the signature behaviors of an active fluid. In particular, the active spheres undergo nonequilibrium clustering (Fig. 1) similar to other model active systems [3,20,21,30].

We establish that this clustering is indeed athermal phase separation by measuring the density in each phase at different parameter values [Fig. 2(a)]. We observe a binodal envelope beyond which the system separates into two phases whose densities collapse onto a single coexistence curve which is a function of activity alone. The phase diagram is thus analogous to that of an equilibrium system
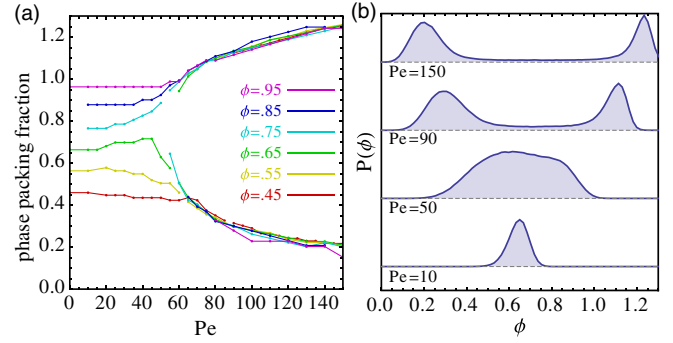

FIG. 2 (color online). (a) Phase densities as a function of Péclet number (Pe) for a range of overall ϕ. At low Pe the system is single-phase, while at increased Pe it phase-separates. The coexistence boundary is analogous to the binodal curve of an equilibrium fluid, with Pe acting as an attraction strength. (b) Observed density distributions for various Péclet numbers. In the single-phase region below $\text{Pe} \approx 50$, $P(\phi)$ is peaked about the overall system density (here $\phi = 0.65$). It broadens and flattens as the critical point is approached, and becomes bimodal as the system phase separates.

of mutually attracting particles undergoing phase separation, with Pe (playing the role of an attraction strength) as the control parameter. This surprising result contradicts the expectation that increased activity will destabilize aggregates and suppress phase separation (as seen in Ref. [31]) and indicates that the effects of activity cannot be described by an "effective temperature" in this system.

Additionally, we identify a critical point at the apex of the bimodal (near $\text{Pe} = 50$, $\phi = 0.7$). In the vicinity of this point, the system exhibits equilibriumlike critical phenomena which will be detailed in a future publication.

The phase-separated steady state.—To characterize the steady state, we measured the fraction of particles in the dense phase at time 100τ (Fig. 3). In contrast with recent work [22] which placed the phase transition boundary at a constant density, we observe that this cluster fraction is a nontrivial function of the system parameters $f_c(\text{Pe}, \phi)$. To understand this relationship we developed a minimal model in which this function can be found analytically. Let us assume the steady state contains a macroscopic cluster which we take to be close packed. Particles in the cluster are stationary in space but their θ_i continue to evolve diffusively. We treat the gas as homogeneous and isotropic, and assume that a particle colliding with the cluster surface is immediately absorbed.

Within this model, we can write the rate of absorption of particles of orientation θ from the gas phase as $k_{\text{in}}(\theta) = \frac{1}{2\pi}\rho_g v_p \cos\theta$, where ρ_g is the gas number density. Integrating yields the total incoming flux per unit length: $k_{\text{in}} = \frac{\rho_g v_p}{\pi}$. To estimate the rate of evaporation, note that a particle on the cluster surface will remain there so long as its self-propulsion direction remains "below the horizon", i.e., $\hat{\mathbf{n}} \cdot \hat{\boldsymbol{\nu}} < 0$, where $\hat{\mathbf{n}}$ is normal to the surface. When its direction moves above the horizon, it immediately escapes
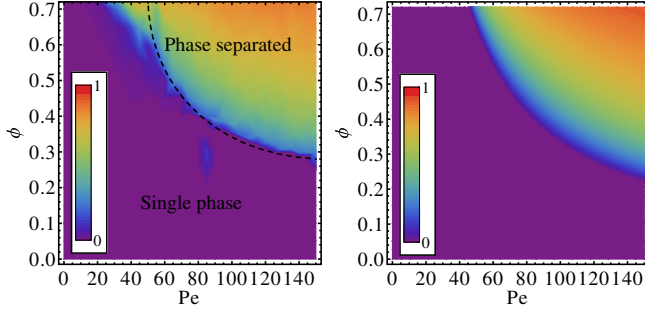
FIG. 3 (color online). Left: contour map of cluster fraction $f_c(\mathrm{Pe}, \phi)$ measured from simulations. The dashed curve marks the approximate location of the binodal. Right: cluster fraction as predicted by our analytic theory [Eq. (3)]. These plots have been restricted to packing fractions that are low enough for the assumptions of our kinetic model to be valid, and for cluster identification to be unambiguous.

and joins the gas. This rate can be calculated by solving the diffusion equation in angular space with absorbing boundaries (for clusters large enough to treat the interface as flat, at $\pm \frac{\pi}{2}$) and initial condition given by the distribution of incident particles: $\partial_t P(\theta, t) = D_r \partial_\theta^2 P(\theta, t)$, with $P(\pm \frac{\pi}{2}, t) = 0$, and $P(\theta, 0) = \frac{1}{2} \cos \theta$. Further, the departure of a surface particle creates a hole through which subsurface particles (whose $\hat{\nu}_i$ may point outwards) can escape. With κ we denote the average total number of particles lost per escape event, which we treat as a fitting parameter. The total outgoing rate is then $k_{\mathrm{out}} = \frac{\kappa D_r}{\sigma}$.

Equating k_{in} and k_{out} yields a steady-state condition for the gas density: $\rho_g = \frac{\pi \kappa D_r}{\sigma v_p}$. ρ_g can be eliminated in favor of f_c, yielding (in terms of our dimensionless parameters),

$$f_c = \frac{4\phi \mathrm{Pe} - 3\pi^2 \kappa}{4\phi \mathrm{Pe} - 6\sqrt{3}\pi\kappa\phi}. \qquad (3)$$

This function is plotted in Fig. 3 with $\kappa = 4.5$, in good accord with our simulation results. Further, the condition $f_c = 0$ allows us to deduce a criterion for the onset of clustering. Restoring dimensional quantities, this condition gives $\phi\sigma v_p \sim D_r$. Note that $\phi\sigma v_p$ is a collision frequency; thus, the system begins to cluster at parameters for which the collision time becomes shorter than the rotational diffusion time.

The mechanism we have presented here is purely kinetic and requires only an intuitive picture of local dynamics at the interface. An alternative view has been described by Tailleur and Cates [32,33] who subsume all interactions into a density-dependent propulsion velocity $v(\rho)$ which decreases with density as collisions become more frequent. From this they construct an effective free energy which shows an instability in the homogeneous phase if $v(\rho)$ falls quickly enough. In a sense our kinetic model represents an extreme case of this picture in which $v(\rho)$ contains a step function such that free particles are noninteracting, and

particles in a cluster are completely trapped (see Fig. S7 in the Supplemental Material [34]).

Structure of the dense phase.—Since the system is composed of monodisperse spheres, the dense phase is susceptible to crystallization [35]. As shown in Fig. 1 the static structure factor of the cluster interior shows a liquidlike isotropy at low Pe, but develops strong sixfold symmetry as activity is increased. Further, the radial distribution function shows clear peaks at the sites of a hexagonal lattice (see Fig. S6 in the Supplemental Material [34]) which sharpen and increase in number as Pe is raised. We also measured the bond-orientational order parameter $q_6(i) = \frac{1}{|\mathcal{N}(i)|} \sum_{j \in \mathcal{N}(i)} e^{i 6 \theta_{ij}}$, where $\mathcal{N}(i)$ runs over the neighbors of particle i (defined as being closer than a threshold distance), and θ_{ij} is the angle between the i-j bond and an arbitrary axis (Fig. 4). We find a structure characterized by large regions of high order with embedded defects that are predominantly 5–7 pairs [Fig. 4(a) inset and S4 in [34]]. Next, we examined the correlation function $\langle q_6^*(r) q_6(r') \rangle$ (Fig. 4) which exhibits a liquidlike exponential decay for systems of low activity, while at higher activity the decay slows to a power law which is indicative of a hexatic [36]. A further transition to a crystal-like plateau is observable in larger systems (see Fig. 4 and S9 and S10 in the Supplemental Material [34]). In all cases, this material is unique in that it is held together by active forces alone, and that the arrest of motion is due to frustration. In this sense it is similar to amorphous materials such as granular packs as reflected by the highly heterogeneous stress distribution (Fig. 1) [37].

Dynamics in the dense phase.—Within the active solid material, self-propulsion forces continuously evolve by rotational diffusion, breaking local force balance and leading to defect formation and migration (see S4 in [34]).
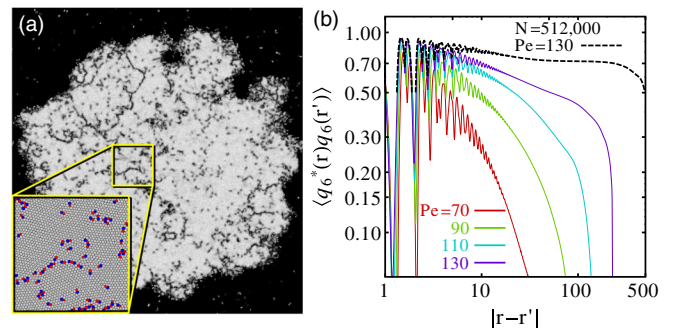

FIG. 4 (color online). (a) Defect structures in a large cluster. Regions of high crystalline order (white) coexist with isolated and linear defects (dark). The color of each particle indicates its $|q_6|$. Inset shows pairs of 5/7 defects. (b) Log-log plot of the correlation function $\langle q_6^*(r) q_6(r') \rangle$ for clusters at various Péclet numbers in systems with $N = 128\,000$, showing a transition from liquidlike exponential to hexaticlike power-law decay as activity is increased. For systems with $N = 512\,000$ (black dashed line), a crystal-like plateau is also observed.
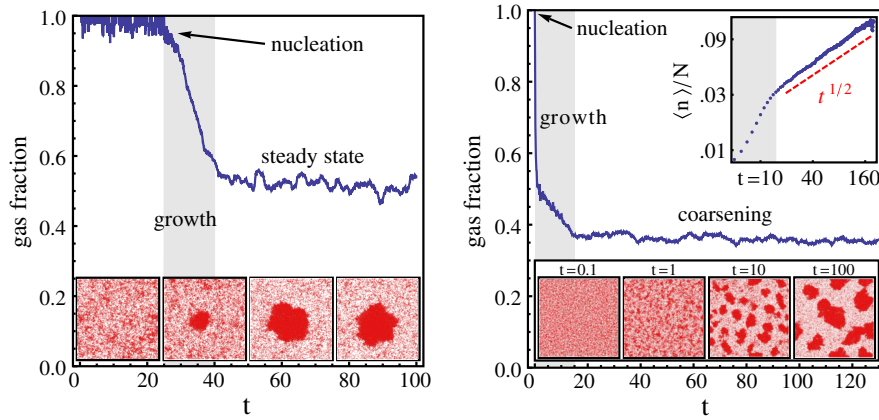
FIG. 5 (color online).   Examples of phase separation kinetics. Left: a system with Pe = 100, ϕ = 0.45 in which a delayed nucleation event leads quickly to steady state. For shallowly quenched systems, the nucleation time can be long enough that artificial seeding is needed to make nucleation computationally accessible. Right: a system with Pe = 80, ϕ = 0.6 where spinodal decomposition leads to a coarsening regime which slowly evolves toward steady state. Inset shows mean cluster size scaling approximately as $t^{(1/2)}$ (see S1 and S8 in the Supplemental Material [34]).

A compelling way to view the motion produced by this athermal process is a process is a simulated fluorescence recovery after photobleaching (FRAP) experiment [38], in which particles within a contiguous region are tagged, making subsequent mingling of tagged and untagged particles visible (see S3 in the Supplemental Material [34]). To quantify this behavior, we measured the mean square displacement (MSD) of particles in the cluster interior. As shown in Fig. 1, we observe subdiffusive motion on short time scales, followed by a superdiffusive regime, returning to diffusive motion on long time scales. The exponents of the subdiffusive and superdiffusive motion ($\frac{1}{2}$ and $\frac{3}{2}$, respectively) are well-conserved across a wide range of propulsion strengths. Note that an isolated self-propelled particle will exhibit diffusive, ballistic, and diffusive behavior on time scales $t < \frac{4D}{v_p^2}$, $\frac{4D}{v_p^2} < t < \frac{1}{D_r}$ and $t > \frac{1}{D_r}$, respectively (see Fig. S5 in [34]). These dynamical regimes are modified by the active solid environment; in particular, the ballistic regime is modulated by "sticking" events as the particle is localized in crystal domains, resulting in the observed Lévy-flight-like behavior [39,40].

Kinetics of phase separation.—Despite the athermal origins of phase separation in this system, simulations quenched to parameters within the binodal curve experience familiar phase separation kinetics (Fig. 5). Systems quenched close to the binodal exhibit a nucleation delay which can be long enough that artificial seeding is necessary for phase separation to be computationally accessible. Systems quenched more deeply undergo spinodal decomposition, leading to a coarsening regime in which the mean cluster size scales surprisingly as $t^{(1/2)}$, with a corresponding length scale $\mathcal{L}(t) \sim t^{(1/4)}$ (Fig. 5 inset, also see S8 in the Supplemental Material [34]). This differs from the standard 2D coarsening exponents, but matches recent simulation results for the Vicsek model and related active systems

[41]. This result should be viewed as preliminary due to the limited range of our data, but nevertheless this unexpected similarity between the coarsening of point-particles with polar alignment and that of spheres with no alignment suggests a deep relationship between these very different types of systems. Future work is needed to uncover the origins of these scaling exponents and their implications for universality in active fluids.

Summary.—A fluid of self-propelled colloidal spheres exhibits the athermal phase separation that is intrinsic to active fluids and is a primary mechanism leading to emergent structures in diverse systems [2,25]. We have shown that the physics underlying this phase behavior can be understood in terms of microscopic parameters. From a practical perspective, our simulations show that the active solid dense phase exhibits a combination of structural and transport properties not achievable in a traditional passive material. Further development of experimental realizations of this system (e.g., Ref. [23]) will advance the development of materials whose phase behavior, rheology, and transport properties can be precisely controlled by activity level.

*hagan@brandeis.edu
†aparna@brandeis.edu

[1] T. Vicsek and A. Zafeiris, Phys. Rep. **517,** 71 (2012).
[2] A. Gopinath, M. F. Hagan, M. C. Marchetti, and A. Baskaran, Phys. Rev. B **85,** 061903 (2012).
[3] F. Peruani, A. Deutsch, and M. Bär, Phys. Rev. E **74,** 030904 (2006).

[4] S. Ramaswamy, R. A. Simha, and J. Toner, Europhys. Lett. **62**, 196 (2003).

[5] L. Giomi, T. B. Liverpool, and M. C. Marchetti, Phys. Rev. E **81**, 051908 (2010).

[6] D. Saintillan, Phys. Rev. E **81**, 056307 (2010).

[7] M. E. Cates, S. M. Fielding, D. Marenduzzo, E. Orlandini, and J. M. Yeomans, Phys. Rev. Lett. **101**, 068102 (2008).

[8] T. Shen and P. G. Wolynes, Proc. Natl. Acad. Sci. U.S.A. **101**, 8547 (2004).

[9] J. Palacci, C. Cottin-Bizonne, C. Ybert, and L. Bocquet, Phys. Rev. Lett. **105**, 088304 (2010).

[10] W. F. Paxton, K. C. Kistler, C. C. Olmeda, A. Sen, S. K. St. Angelo, Y. Cao, T. E. Mallouk, P. E. Lammert, and V. H. Crespi, J. Am. Chem. Soc. **126**, 13424 (2004).

[11] Y. Hong, N. M. K. Blackman, N. D. Kopp, A. Sen, and D. Velegol, Phys. Rev. Lett. **99**, 178103 (2007).

[12] H.-R. Jiang, N. Yoshinaga, and M. Sano, Phys. Rev. Lett. **105**, 268302 (2010).

[13] G. Volpe, I. Buttinoni, D. Vogt, H.-J. Kummerer, and C. Bechinger, Soft Matter **7**, 8810 (2011).

[14] V. Narayan, S. Ramaswamy, and N. Menon, Science **317**, 105 (2007).

[15] A. Kudrolli, G. Lumay, D. Volfson, and L. S. Tsimring, Phys. Rev. Lett. **100**, 058001 (2008).

[16] J. Deseigne, O. Dauchot, and H. Chaté, Phys. Rev. Lett. **105**, 098001 (2010).

[17] A. Baskaran and M. C. Marchetti, Phys. Rev. E **77**, 011920 (2008).

[18] A. Baskaran and M. C. Marchetti, Phys. Rev. Lett. **101**, 268101 (2008).

[19] F. Peruani, T. Klauss, A. Deutsch, and A. Voss-Boehme, Phys. Rev. Lett. **106**, 128101 (2011).

[20] Y. Yang, V. Marceau, and G. Gompper, Phys. Rev. E **82**, 031904 (2010).

[21] S. R. McCandlish, A. Baskaran, and M. F. Hagan, Soft Matter **8**, 2527 (2012).

[22] Y. Fily and M. C. Marchetti, Phys. Rev. Lett. **108**, 235702 (2012).

[23] I. Theurkauff, C. Cottin-Bizonne, J. Palacci, C. Ybert, and L. Bocquet, Phys. Rev. Lett. **108**, 268303 (2012).

[24] S. Mishra and S. Ramaswamy, Phys. Rev. Lett. **97**, 090602 (2006).

[25] M. E. Cates, D. Marenduzzo, I. Pagonabarraga, and J. Tailleur, Proc. Natl. Acad. Sci. U.S.A. **107**, 11715 (2010).

[26] Y. Peng, Z. Wang, A. M. Alsayed, A. G. Yodh, and Y. Han, Phys. Rev. Lett. **104**, 205703 (2010).

[27] Y. Han, N. Y. Ha, A. M. Alsayed, and A. G. Yodh, Phys. Rev. E **77**, 041406 (2008).

[28] J. D. Weeks, D. Chandler, and H. C. Andersen, J. Chem. Phys. **54**, 5237 (1971).

[29] A. C. Brańka and D. M. Heyes, Phys. Rev. E **60**, 2381 (1999).

[30] H. Chaté, F. Ginelli, G. Grégoire, F. Peruani, and F. Raynaud, Eur. Phys. J. B **64**, 451 (2008).

[31] J. Schwarz-Linek, C. Valeriani, A. Cacciuto, M. E. Cates, D. Marenduzzo, A. N. Morozov, and W. C. K. Poon, Proc. Natl. Acad. Sci. U.S.A. **109**, 4052 (2012).

[32] J. Tailleur and M. E. Cates, Phys. Rev. Lett. **100**, 218103 (2008).

[33] M. E. Cates and J. Tailleur, arXiv:1206.1805.

[34] See Supplemental Material at http://link.aps.org/supplemental/10.1103/PhysRevLett.110.055701 for movies and additional figures.

[35] J. Bialké, T. Speck, and H. Löwen, Phys. Rev. Lett. **108**, 168301 (2012).

[36] D. R. Nelson, *Defects and Geometry in Condensed Matter Physics* (Cambridge University Press, Cambridge, England, 2002).

[37] R. Blumenfeld and S. F. Edwards, J. Phys. Chem. B **113**, 3981 (2009).

[38] A. van Blaaderen, J. Peetermans, G. Maret, and J. K. G. Dhont, J. Chem. Phys. **96**, 4591 (1992).

[39] J. Klafter, M. F. Shlesinger, and G. Zumofen, Phys. Today **49**, No. 2, 33 (1996).

[40] G. Pfister and H. Scher, Adv. Phys. **27**, 747 (1978).

[41] S. Dey, D. Das, and R. Rajesh, Phys. Rev. Lett. **108**, 238001 (2012).